ASSESSMENT OF CLIMATE VARIABILITY OF THE GREENLAND ICE SHEET: INTEGRATION OF IN SITU AND SATELLITE DATA

K. Steffen, W. Abdalati, J. Stroeve, J. Key
University of Colorado at Boulder
Cooperative Institute for Research in Environmental Sciences
Division of Cryospheric and Polar Processes
Campus Box 216, Boulder CO 80309

NAGW-2158
Annual Progress Report
to
National Aeronautics and Space Administration

January 1994

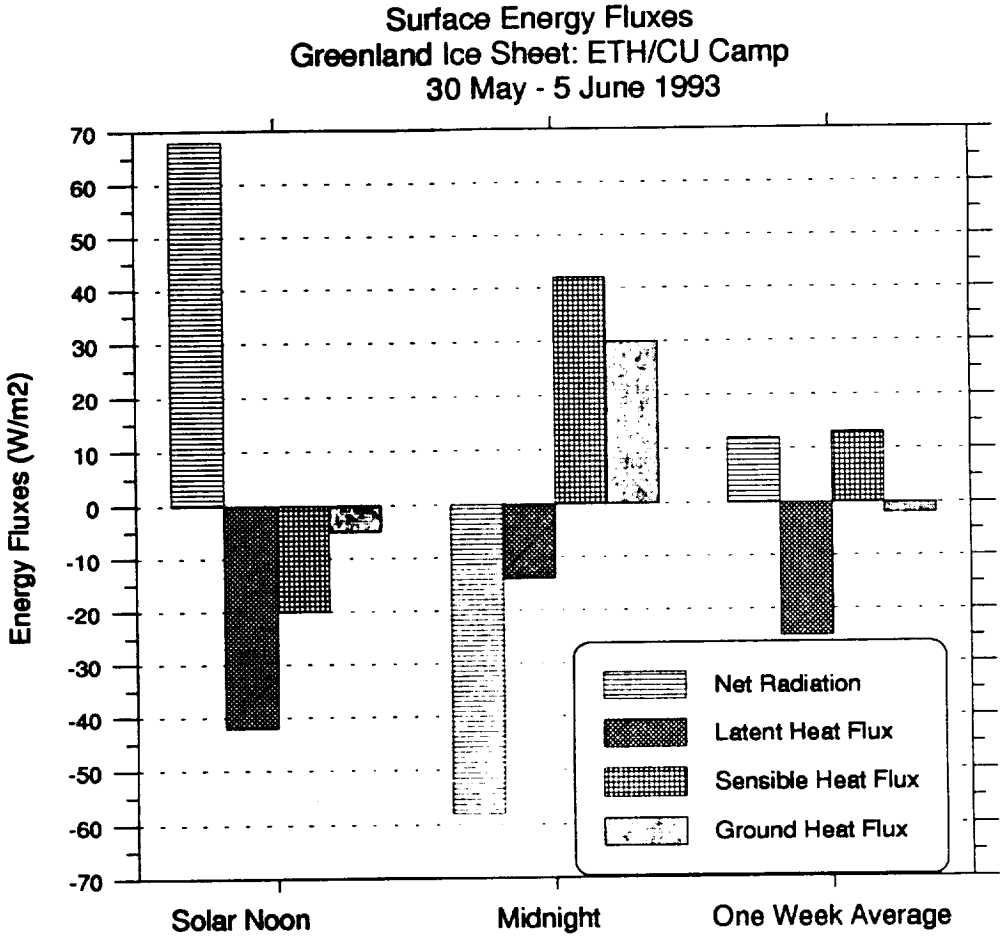

University of Colorado at Boulder

Konrad Steffen

Cooperative Institute for Research in Environmental Sciences

CIRES, Campus Box 216
Boulder, Colorado 80309-0216
U.S.A.

Tel (303) 492 4524
Fax (303) 492 1149
Telex 7402872 Koni UC

Bitnet koni@seaice.colorado.edu
Telemail K.Steffen/Omnet

Boulder, February 10, 1994

NASA Scientific & Technical Information Facility
P.O. Box 8757
Baltimore/Washington International Airport
Maryland 21240

Please find enclosed two copies of the progress report and reprints for the NASA Grant NAGW-2158.

Yours sincerely

Konrad Steffen
Prof. and Fellow

TABLE OF CONTENTS

SUMMARY

In 1993 we completed a successful field season at the CU/ETH camp on the Greenland Ice Sheet. The major accomplishments were:

- Retrieval of 298 days of climate and glaciological data recorded in our absence.
- A suite of climate measurements were collected for approximately 6 weeks period, which included all components of the radiation, turbulent fluxes, temperature - humidity - wind profiles, snow ablation, water content, grain size and density of the snow pack, spectral directional and hemispherical reflectance.
- Forty satellite images were collected during the 1993 field season.
- A total of 21 radiosondes were launches coincidentally with the satellite overpasses.

Data analysis showed the following results:

- The energy flux balance during the pre-melt period showed that on the average the latent heat flux was the only energy sink, and responsible for the sublimation of 1 mm water equivalent of snow per day.
- A relationship between narrow-band and broad-band albedo was derived for the surface with an rms error of 0.74 %.
- A surface albedo accuracy of 0.1 % for channel 1 and 13 % for channel 2 was achieved for AVHRR based on radiative transfer model and radiosonde data as input.
- Clear sky optical depth of 0.15 for the AVHRR 550 - 700 nm wavelength range were typical during the spring months.
- Radiative transfer modeling of the firn supports our beliefs that the observed trends in 18 and 19 GHz passive microwave brightness temperatures are attributable to accumulation rates changes.
- Modeling also indicates the above relationship is detectable because of the presence of depth hoar.
- Snow melt can be detected by a distinct signal in the passive microwave gradient ratio (GR) and has been used for wet/dry snow classification with a threshold at GR = 0.025.
- The relationship between brightness temperature and accumulation rates is not well established in Antarctica due to the small snow grain growth rate and low accumulation values.

The 1994 objectives include:

- Statistical analysis of grain size distribution using the serial sieving method combined with photomicrography.
- Detailed investigation of snow soot content as an input parameter for the reflectance modeling.
- Study the change and penetration depth of passive microwave radiation throughout the transition of dry to wet snow with an active radar on site.
- Extend radiative transfer model to represent 37 GHz channels in order to quantify snow accumulation rate estimates

1. INTRODUCTION

1.1 Rationale of the Study

The proposed research involves the application of multispectral satellite data in combination with ground truth measurements to monitor surface properties of the Greenland Ice Sheet which are essential for describing the energy and mass of the ice sheet. Several key components of the energy balance are parameterized using satellite data and *in situ* measurements. The analysis will be done for a ten year time period in order to get statistics on the seasonal and interannual variations of the surface processes and the climatology.

Our goal is to investigate to what accuracy and over what geographic areas large scale snow properties and radiative fluxes can be derived based upon a combination of available remote sensing and meteorological data sets. Operational satellite sensors are calibrated based on ground measurements and atmospheric modeling prior to large scale analysis to ensure the quality of the satellite data. Further, several satellite sensors of different spatial and spectral resolution are intercompared to access the parameter accuracy. Proposed parameterization schemes to derive key component of the energy balance from satellite data are validated. For the understanding of the surface processes a field program was designed to collect information on spectral albedo, specular reflectance, soot content, grain size and the physical properties of different snow types. Further, the radiative and turbulent fluxes at the ice/snow surface are monitored for the parameterization and interpretation of the satellite data.

The expected results include several baseline data sets of albedo, surface temperature, radiative fluxes, and different snow types of the entire Greenland Ice Sheet. These climatological data sets will be of potential use for climate sensitivity studies in the context of future climate change.

1.2 Logistic Summary

We arrived at the CU/ETH Greenland station on May 22 1993. The first three days on the station were spent snow shoveling to completely uncover the station and getting the station in running order. On May 26, 330 GMT the climate tower was completely hooked up and providing the following data:

1. wind speed at three levels
2. temperature at three levels
3. relative humidity at three levels
4. wind speed and direction at one level
5. incoming short wave radiation at one level
6. reflected short wave radiation at one level
7. incoming long wave radiation at one level
8. net radiation at one level
9. barometric pressure

The initial height of the three levels was 54 cm, 104 cm, and 204 cm as measured from the surface of the ice sheet. The wind direction sensor was at a height of 340 cm. Final levels were at 60 cm, 110 cm, and 210 cm.

The orientation of the tower was as follows:

1. Profile arms, from which temperature, relative humidity, and wind speed were mounted, were oriented 74 degrees from magnetic north.
2. The pyrgeometer, which measured incoming long wave radiation, was oriented 14 degrees from magnetic north.
3. Pyranometer number 1, which measured incoming short wave radiation, was oriented 250 degrees from magnetic north.
4. Pyranometer number 2, which measured reflected short wave radiation, was oriented 168 degrees from magnetic north.
5. The net radiometer was oriented 230 degrees from magnetic north.

The climate tower provided continuous profile data at three levels of wind speed, temperature, and relative humidity. Also measured were wind direction, pressure, net radiation, incoming short wave and long wave radiation, and reflected shortwave radiation beginning May 26 at 0330 GMT ending June 09 0200 GMT, and from June 10 1830 GMT to June 20 2220 GMT (Fig. 1.1). During the period from June 09 230 GMT to June 10 1600 GMT a relative calibration was performed for the temperature, relative humidity and wind speed sensors. This calibration was repeated on June 20. On June 21, 1409 GMT, the calibration began for the pyranometers.

In addition to the evaluation of fluxes using the aerodynamic (profile) method, we measured the convective fluxes using the eddy fluctuation method. This involved the following instruments:

1. Lyma Alpha Hygrometer
2. Sonic anemometer and fine wire thermocouple
3. Net radiometer
4. Barometric pressure sensor
5. Relative humidity and temperature sensor

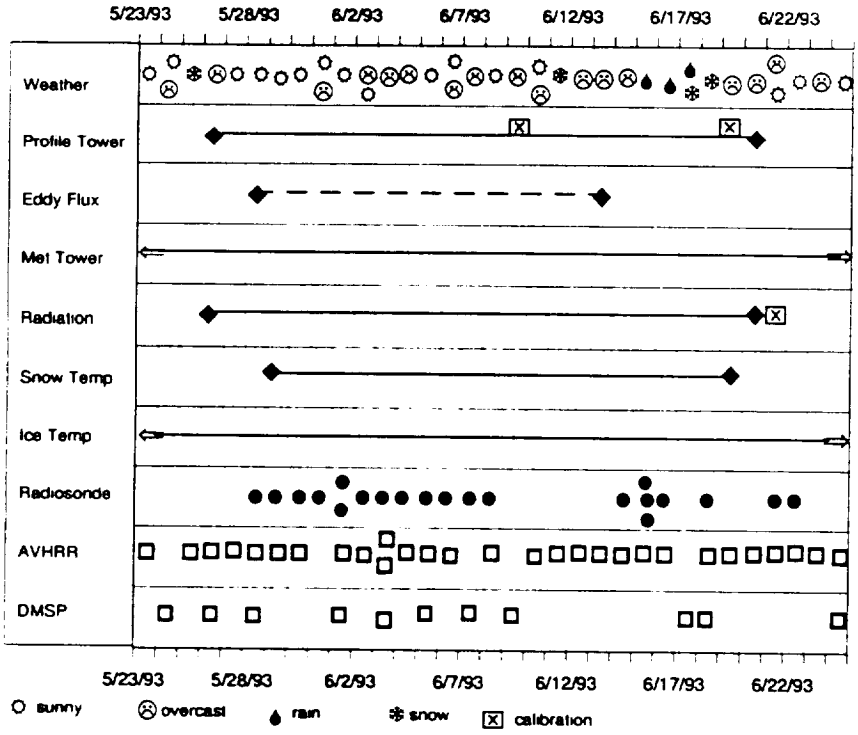

Fig. 1.1 Time line of the CU/ETH Camp activities

2. SURFACE CLIMATOLOGY

2.1 Winter 92/93 Record

The automatic weather station at the CU/ETH camp was programmed in summer, 1992 to record climatological data throughout the winter. Two Campbell 21X dataloggers were used for the recording which were powered by a 280 Ah battery pack. One datalogger collected mean wind speed, maximum wind speed within the recording interval, mean wind direction, mean air temperature at 10 m height, and 13 ice temperatures down to 10 m depth in the ice sheet. The meteorological data was recorded at three hour intervals and the ice temperatures were recorded once a day. A second data logger was used as a back-up unit with which an identical set of meteorological parameters was recorded.

The first data logger recorded all parameters from July 28, 1992 for 298 days until the station was re-occupied on May 22, 1993. The second data logger failed recording after 140 days due to malfunction of the recording unit (memory allocation error). However, no climate data was lost because both units, including the sensors, were operated separately. The air temperature was close to the freezing point when the station was occupied in spring 1993. Fig. 2.1 shows the distinct diurnal cycle of the air temperature and the abrupt change between the winter condition with a mean temperature around -25° C and the spring/summer condition close to the freezing point within three days only.

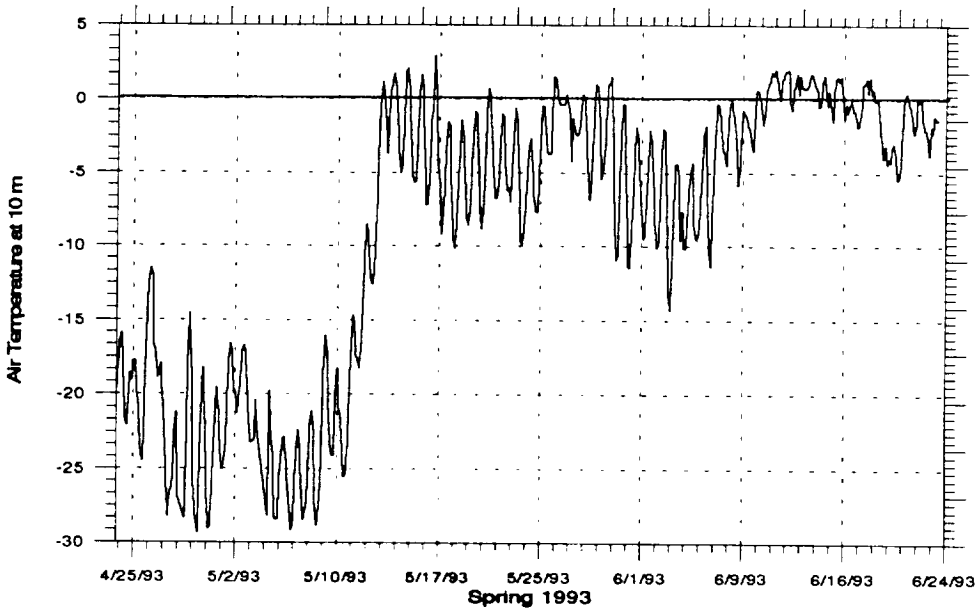

Fig. 2.1 Air temperature record at 10 m above the ice surface

The winter climate data is summarized in Figures 2.2 and 2.3. It is interesting to note the large temperature variations throughout the winter of up to 40° C occurring in less than one day. The large temperature increase correlates well with the occurrence of high surface winds which can be attributed to the adiabatic heating of dry air descending from higher elevations of the Greenland Ice Sheet (Foehn type wind). The average wind speed during the 10 months (July 92 - March 93) at the CU/ETH stations was 10.1 ms^{-1} with a maximum wind speed of 30.0 ms^{-1}. The average air temperature for the same time period was -17.2° C with a minimum reading at -47.2° C for the three-hour mean. Temperatures close to the freezing point occurred several time during the winter which explains the thin ice layers in the winter snow accumulation.

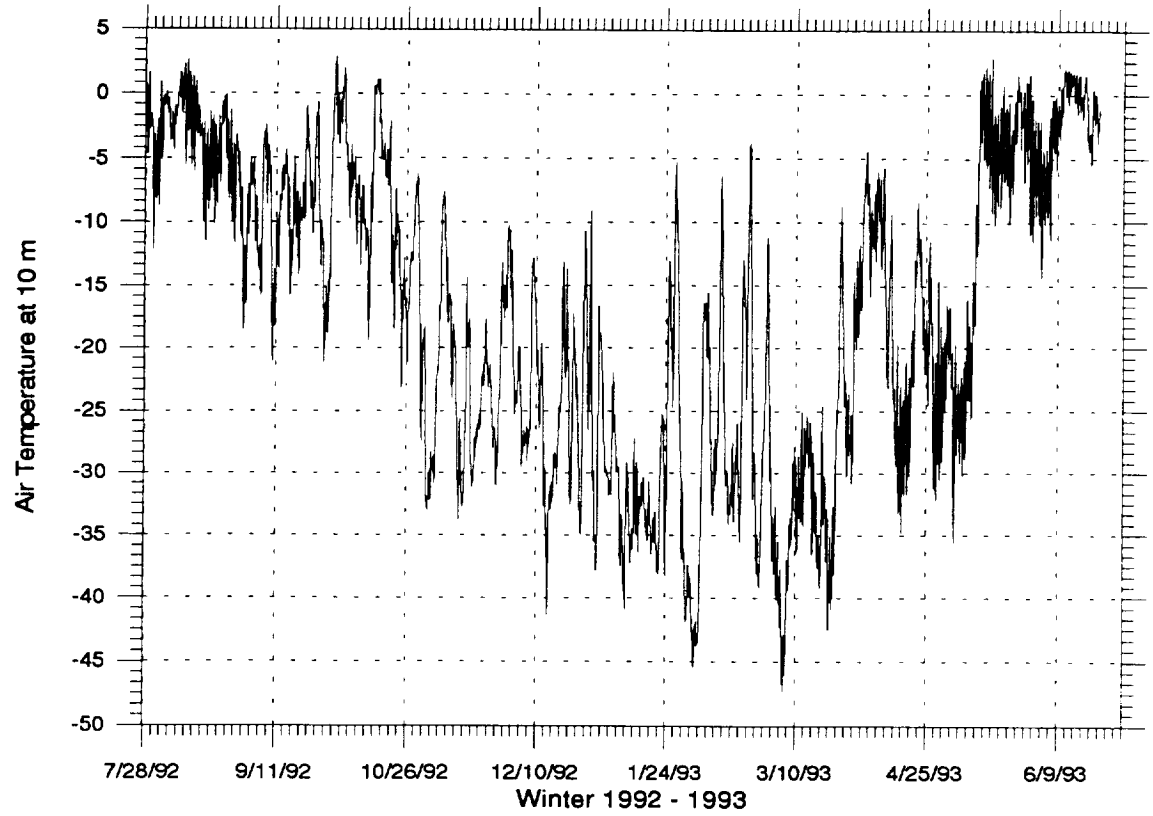

Fig. 2.2 Winter 92/93 temperature recorded for the CU/ETH station

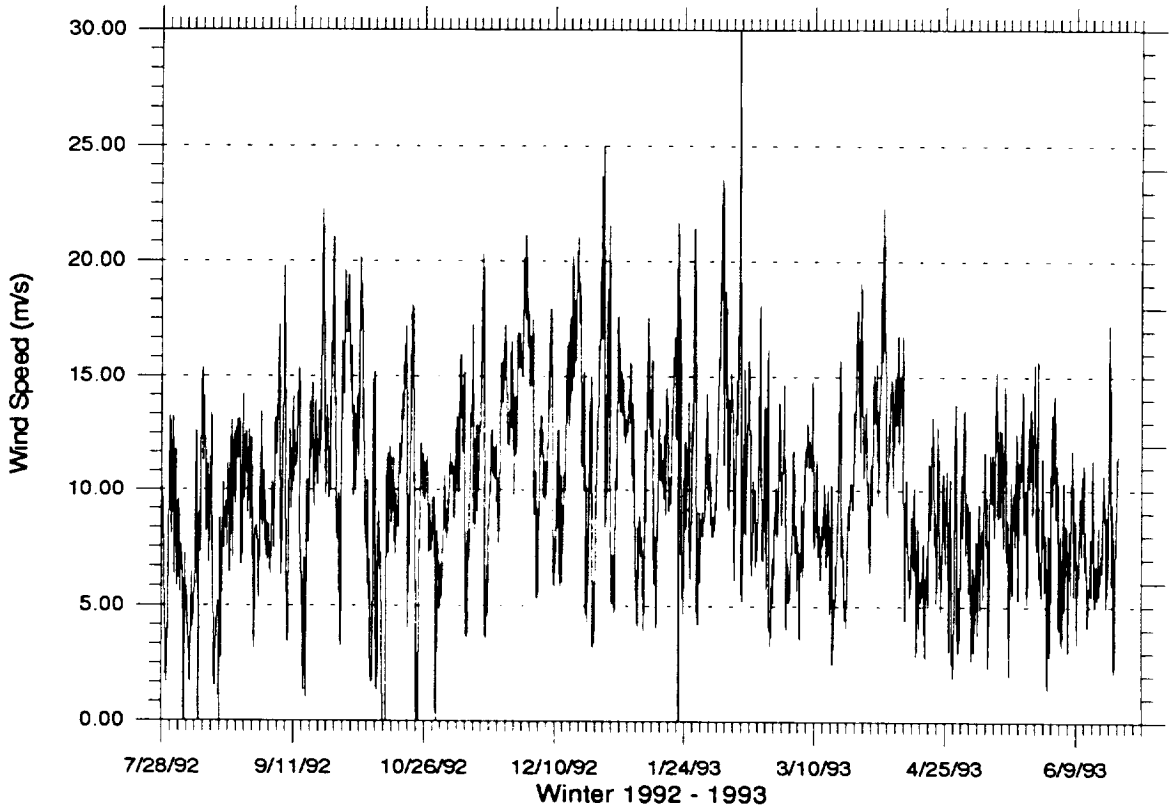

Fig. 2.3 Winter 92/93 wind record for the CU/ETH station.

2.2 *Surface Energy Balance*

The surface energy balance was measured using the aerodynamic (profile) method and the eddy fluctuation method. The instrumentation of the methods are described in Chapter 1.2. Results from the eddy fluctuation method are given below.

The net radiation showed a large diurnal cycle between -60 Wm^{-2} around midnight and 70 Wm^{-2} at noon (Fig. 2.4). On the average between May 30 and June 5 the net radiation was in surplus by 12 Wm^{-2} (see cover diagram from this report). The sensible heat flux showed also a strong diurnal cycle with negative values (heat sink) at noon and a large heat source during the night. The latent heat was negative throughout the whole week with values around -40 Wm^{-2} at noon. The average energy that was used for the sublimation of snow over one week was -20 Wm^{-2}, which equals to an average evaporation/sublimation rate of 1 mm water equivalent of snow per day. Apparently the evaporation at the equilibrium line altitude can be quite substantial, especially under Foehn condition, and they compare well with evaporation rates of 1.3 mm W.E. measured at the Inland Ice at 460 m elevation (Orvig, 1970). The ground heat flux of -1.9 Wm^{-2} was derived as an residual for the energy balance. The measured ground heat flux derived from temperature measurements in the snow is presented in Chapter 4.2.

During the premelt period the latent energy flux (sublimation of snow) is the only energy sink with an average value of 2.16 $MJm^{-2}d^{-1}$. Net radiation and sensible heat flux are both energy sources with approximately the same value of about 1.2 $MJm^{-2}d^{-1}$ about 1.2 $MJm^{-2}d^{-1}$ over a one week period during premelt (see Fig. on cover of this report). The ground heat flux as derived with the temperature probes was 0.14 $MJm^{-2}d^{-1}$, and the value derived as a residual of the eddy flux method was -0.17 $MJm^{-2}d^{-1}$.

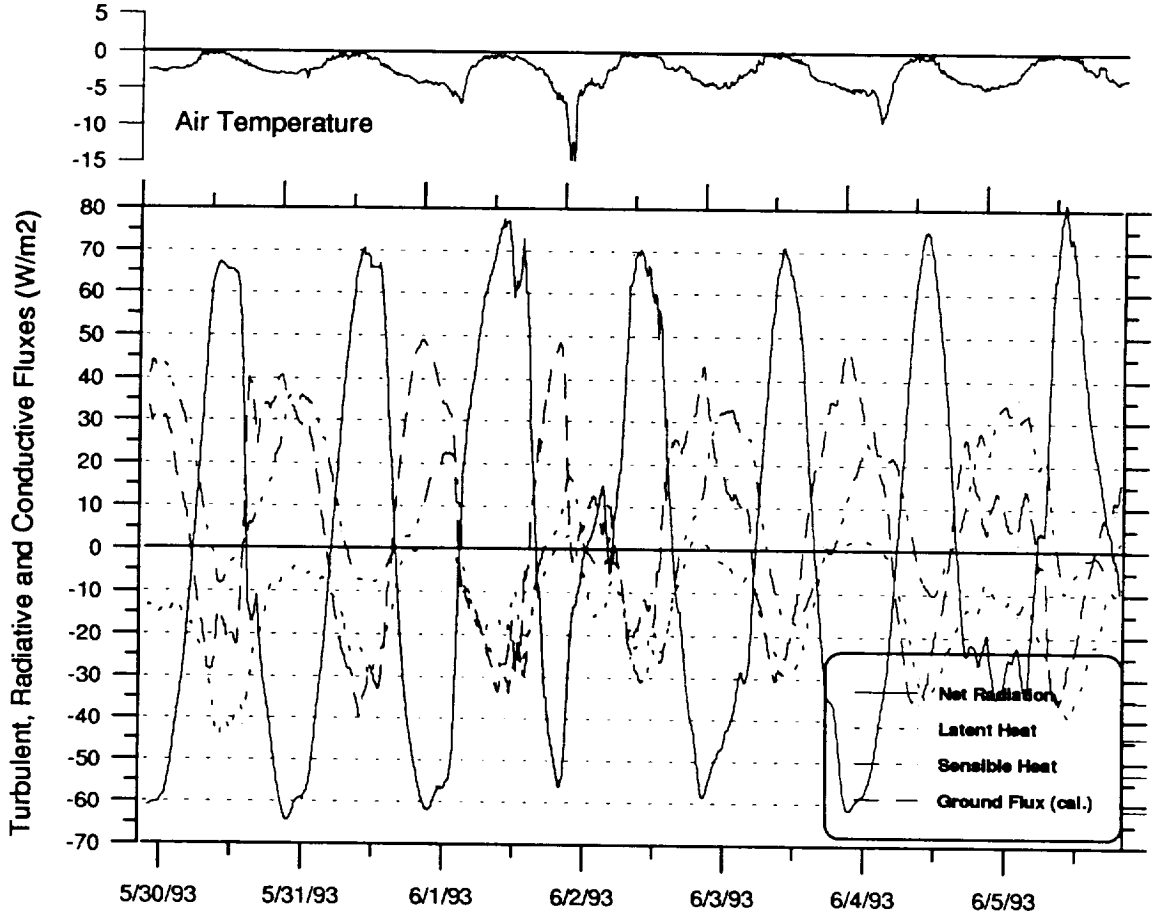

Figure 2.4 Energy balance at the snow surface

2.3 Ablation Measurements

Daily snow ablation measurements were made beginning May 30, at 1900 GMT. By planting 4 bamboo poles in the snow, side by side spaced approximately 20 m apart, a snowline datum was established. The snowdepths was determined at each pole by measuring the distance from the snow surface to the ice below at four locations around each pole and taking their average. Initially measurements were made twice daily until June 2 at around 1400 and 2000 GMT after which they were made only once a day at around 2000 GMT until June 23.

From the measurements we find the snow was slowly melting from May 30 to June 09 with a total amount of ablation of 2.8 cm. During this time period the average temperature was -4.2° C and the diurnal temperature range decreased from about 10° C (nighttime lows of approximately -9° C to -14° C and daytime highs of approximately -3° C to 3° C) to about 5° C (nighttime lows of approximately -3° C and daytime highs of approximately 2° C) during the period of June 5 to June 9. Between June 9 and June 17 temperatures were warm temperatures (average of 1.3° C), the skies were mostly overcast, with some light snow/rain beginning on June 15 around 1500 GMT and continuing off and on through June 17. During this time period the ablation steadily increased to a total of 17.5 cm. On June 17 and June 18 we had a 4-5 cm total increase in snow due to blowing snow and some snow precipitation. The total amount of ablation at the end of the measurement period was 22.7 cm.

3. SURFACE AND PLANETARY ALBEDO

The variation of solar radiation absorbed and reflected by the earth is a key factor in the understanding of climate change. Due to the large size of the Greenland Ice Sheet, satellite data is the only practical source of data for long term monitoring of the seasonal and interannual variations of the surface as well as the planetary albedo. Thus, during the 1993 field season we proceeded to make surface measurements for validation of albedos derived from satellite sensors such as the NOAA Advanced Very High Resolution Radiometer (AVHRR). A total of 29 AVHRR and 11 DMSP OLS images were acquired during the 1993 field season (Fig. 1.1).

3.1 Broad-Band Albedo Parameterization

For climatological purposes, it is desirable to employ an albedo measurement that represents the surface reflectance as well as the earth-atmosphere system reflectance integrated over the entire spectrum. This is usually referred to as broad-band albedo. The AVHRR multispectral narrow-band radiometric scanners, with their small fields of view only measure the reflectance in a few narrow-band channels and need proper adjustments so that these data can be used to estimate broad-band albedo values.

For top of the atmosphere (TOA) planetary albedo estimates, correction schemes already exist for the visible and near IR wavelength bands for the NOAA AVHRR satellites. One such correction scheme is based on a multivariate regression analysis of the Nimbus-7 earth radiation broad-band data and AVHRR narrow-band data (Wydick et al., 1987). However, this statistical approach was done for NOAA-7 and still needs to be determined for the NOAA satellites 8 through 12. Li and Leighton (1992) did a similar regression analysis but unlike Wydick, they used data sets collected on the same platform, thereby ensuring a higher degree of coincidence and collocation.

However, for surface broad-band albedo estimates derived from satellite data, we cannot apply the same relationship that is used in obtaining planetary albedos since there are different atmospheric attenuations in the two AVHRR channels. Therefore, we need to derive the relationship between narrow-band and broad-band albedo based on surface estimates. This was a goal of the 1993 field season.

For the conversion, we made daily spectrometer measurements during the 1993 field season to coincide with the time of the satellite overpass so that we would have coincidental measurements. From these spectrometer measurements, the narrow-band albedos representing the NOAA-12 AVHRR channel 1 (570-700 nm) and channel 2 (725-975 nm) wavelength regions were extracted.

In addition to the spectrometer measurements, broad-band reflectances were measured with a set of Eppley Pyranometers as part of the ongoing radiation balance experiment at the CU/ETH camp. Using twopyranometers, one up looking, the other down looking, the surface broad-band albedo was measured. The relative accuracy of the albedo values is estimated to be 0.7% (Haefliger et al., 1993) which is expected using two different kinds of instruments. Fig. 3.1 shows the relation between the observed broad-band albedo and the narrow-band albedo for AVHRR channel 2 as measrued with the spectrometer.

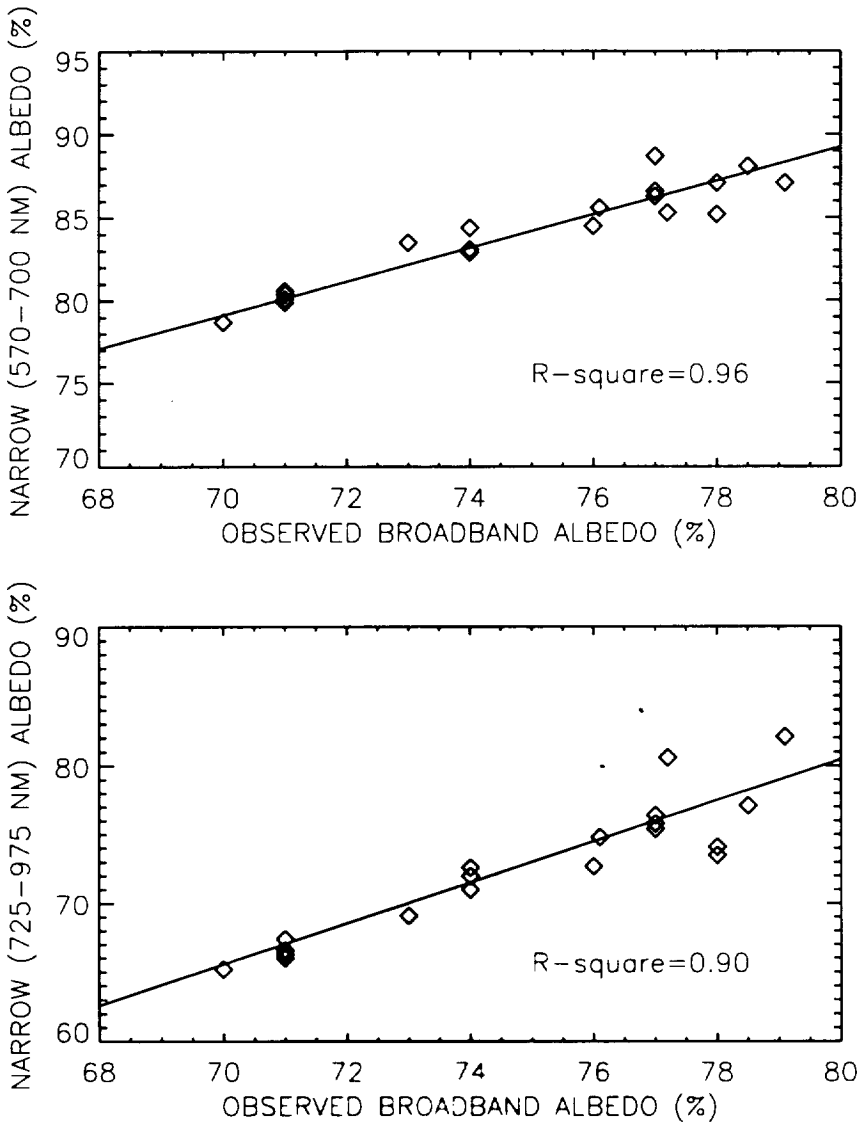

Fig. 3.1 Observed broad-band albedo as measured with the pyranometers versus the narrow-band albedo for the wavelengths region of the AVHRR channels.

Using 31 coincidental broad-band and narrow-band albedos measured at the CU/ETH station on the Greenland Ice Sheet, a linear relationship relating AVHRR channel 1 and channel 2 reflectances to a broad-band surface albedo was derived through a multivariate regression analysis.

$$\alpha = a + b_1 \rho_1 + b_2 \rho_2$$

In the equation, α represents the broad-band albedo, $\rho 1$ and $\rho 2$ represent the NOAA-12 AVHRR channel 1 and channel 2 reflectances respectively, a, b1, b2 are constants.

The overall root mean square (rms) error of the broad-band estimate using this equation is 0.74%. Alternatively, we can also derive a one-parameter model based on the channel 1 wavelength region which results in an overall rms error of 1.01%. The accuracy difference between the two models is similar to the difference Wydick et al. found for snow types in their TOA conversion. For comparison, Li and Leighton's TOA relationship applied to surface broad-band albedo calculation resulted on average of albedos that are about 5% higher than ours.

Future efforts will concentrate on processing all of the spectrometer data from 3 field seasons 1990, 1991 and 1993 in order to derive model parameters for different snow types (e.g. dry snow, onset of melt, wet snow, bare ice)

3.2 AVHRR-Derived Albedo

NOAA-12 AVHRR Local Area Coverage (LAC) data was obtained from the National Satellite Data Service during the period we were at the station (Fig. 1.1). The resolution of the data is 1 km at nadir and decreases with distance from nadir. The data is in level 1B format which includes information for the navigation and calibration of the images. Pre-launch calibration coefficients (Kidwell, 1991) are used to convert the raw data into percent albedo following the description given in the NOAA users guide and includes the non-linear corrections.

In order to correct for the geometric distortions caused by the curvature of the earth and the scanning geometry, the images have been geo-registered and mapped to polar stereographic projection grid using a navigation code developed by Baldwin and Emery (1993). A small registration error is present in the resulting images that can be removed by linearly nudging the images onto a map grid. By doing this the registration errors can be reduced to +/- one half pixel, thereby ensuring the geographical location of the station pixel to be identical between orbits.

In addition, the images were corrected for the solar zenith dependence by dividing by the cosine of the solar zenith angle. To date, four images have been processed and compared with ground measurements. These are May 29, May 30, June 01, and June 08, 1993.

The basis of the use of satellite measurements to determine surface albedo is the assumption that the reflected signal received at the top of the atmosphere is dominated by solar energy reflected from the earth's surface. However, the signal is affected by atmospheric scattering and absorption processes along both the incident and reflected path lengths and therefore, we must correct the satellite data for the intervening atmosphere. Such a correction can be accomplished using a linear relationship between clear sky planetary albedo and surface albedo (Koepke, 1989) or using a radiative transfer model. Several radiative transfer models are available, and one that provides reasonable and accurate atmospheric modeling is the 5S code developed by Tanré and Duhaut (1990. This is one used in our study. Using output from the 5S code we can obtain the parameters necessary to convert the TOA albedos to surface albedos.

To run the code, illumination and observation geometries for the station pixel were provided as input. Daily radiosonde balloon launches that coincided with the satellite overpass provided water vapor input (Fig. 1.1). The aerosol optical depths for the 550-700 nm wavelength range were derived from sunphotometer measurements as discussed in the next section. Ozone concentration was taken to be that of standard subarctic summer.

The resulting surface albedos were then compared with the surface albedos observed on the ground bythe spectrometer. The difference between the measured and calculated narrow-band surface albedo for channel one is about 0.1% for the four days (Fig. 3.2). For channel two the difference between calculated and measured narrow-band albedo is about 13%. The high difference for channel two is thought to be a result of larger sensor degradation for that channel, since comparisons with two other radiative transfer models,

namely LOWTRAN and DISORT, proved similar results. Thus, future work will focus on using a large scale reference area such as that over dry snow for calibration of the sensor.

Using the resulting surface narrow-band albedos derived from satellite, we can then compute the surface broad-band albedo from the relationship derived in section 3.1. Using the two-channel model the resulting broad-band albedo underestimates the station measured surface broad-band albedo by on average by 2.2%. This error is almost completely due to the underestimation of the true narrow-band albedo for channel 2. Alternatively, we can use the one-channel model to compute the surface broad-band albedo, and the error is reduced to less than 1%. However, using the one-channel model doesn't follow the true trend variation in the surface albedo. Thus, we need to combine both channels for a more accurate description of surface albedo variations providing we are accurately able to predict the narrow-band surface albedo for channel 2.

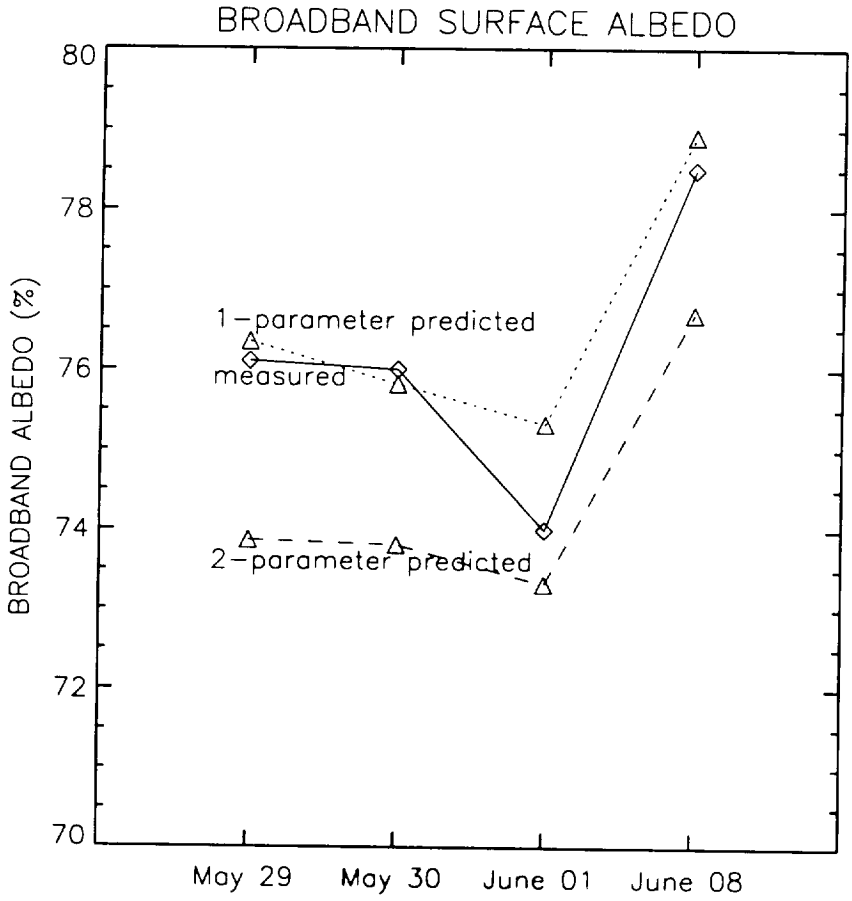

Fig. 3.2 Comparison of measured broad-band surface albedo with AVHRR derived values.

Some of the discrepancy could also be a result of assuming the surface to be Lambertian and neglecting the bidirectional reflectance of a snow surface which can cause a 1-2% error (Steffen, in preparation) for large scanner and solar zenith angles. This is something which will be corrected for in the future. In addition, the accuracy of the 5S radiative transfer model is uncertain, and we need to find a means to validate the transmission values.

3.3 Atmospheric Path Length

The optical depth, (τ) is a spectral quantity directly related to the vertical transmittance (T) to space through the relationship $T = e^{-\tau}$. The optical depth of a mixture of absorbing/scattering molecules and particles is

defined as the sum of the individual scattering and absorption optical paths, $t = t_{sc} + t_a$. The particle, or aerosol component, impacts all visible imagery and is believed to vary significantly in Arctic region (Lindsay and Rothrock, 1993).

At the CU/ETH camp, measurements of the irradiance (I) were made by pointing a sun photometer at the sun. From the Lambert-Beer law we can then solve for the total optical depth by knowing the atmospheric airmass and the calibration factor of the instrument, which is defined by extrapolating the curve of atmospheric airmass vs. natural log of the photometer voltage (Langley plot method, Fig. 3.3) Sun photometer measurement in the wavelength region of 550-700 nm were made daily to coincide with the satellite overpass. This wavelength region was chosen to coincide with the AVHRR channel 1 sensor.

In order to obtain the aerosol optical depth we need to subtract from the total optical depth the contributions due to Rayleigh (molecular) scattering and that due to the absorption by atmospheric gases such as ozone, water vapor, carbon dioxide, etc. To account for the optical depth due to Rayleigh scattering, we used the basic equation (Penndorf, 1957) in which the refractive index of air is computed using Edlen's 1966 formula and Young's recommended value (Young, 1980) for the depolarization factor. In addition, standard conditions were assumed for the columnar and molecular number density. Ozone was the only gas considered in the 550-700 nm wavelength region and was based on the atmospheric ozone amount of 0.4 cm (Iqbal, 1983).

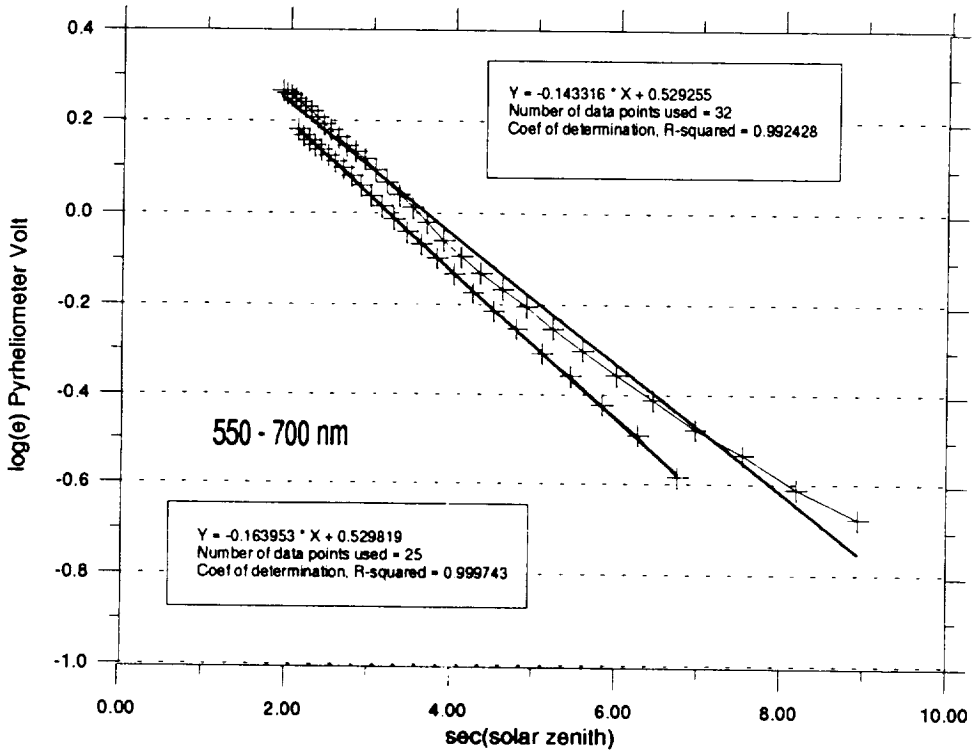

Figure 3.3 *The sun photometer voltage reading in logarithmic scale versus the secance of the solar zenith angle. With the Langley plot method the optical path lengths for the wavelengths region of AVHRR channel 2 can be determined.*

4. SURFACE MELT SIGNATURES

The extent and duration of surface melt of the Greenland Ice Sheet are of critical importance in understanding the Arctic climate, yet they are currently not well known. The increase in water content that occurs when the snow melts results in a reduction of albedo. This lower albedo in turn increases the amount of energy absorbed in the melt areas, which effects both the energy balance and climate in these regions.

When considered over the entire extent of the ice sheet, the impact of melt on the arctic energy balance and climate is of global significance.

For these reasons, accurate assessments of the melt conditions, specifically the dates of melt onset, the dates of refreeze, and a comprehensive assessment of the areas that experience melt, are essential to the understanding of climatological processes and conditions in the Arctic as well as the Antarctic. In addition, trends in the melt processes can all be indicative of trends in the global and local climate. By monitoring the melt parameters mentioned above, changes in the climate of not only Greenland, but potentially the world can be detected.

Satellite remote sensing, particularly passive microwave remote sensing, offers a very promising means of assessing large scale melt occurrences. Because of the existence of a distinct microwave signature at the onset of melt and throughout the melt period, the entire ice sheet can be examined almost daily, and the wet snow regions can be identified and monitored throughout each melt season. Furthermore, between the SMMR and SSM/I data sets, there exists an extended time period of coverage which dates back to October, 1978. Thus, a somewhat comprehensive time series can be examined using passive microwave data.

However, in order for these satellite data to be useful, a certain number of "ground truth" measurements must be made. A limited amount of data exists from previous excursions by scientists from the Swiss Federal Institute of Technology (ETH), however, the refinement of the proposed algorithm for snow melt detection requires additional data. The collection of such data was one of the objectives of this past year's expedition to the ETH/CU research camp.

4.1 Temperature Record in Snow

In order to relate the snow melt to its microwave signature, the snow surface and subsurface temperatures must be measured throughout the melt period. These temperatures are then compared to the corresponding satellite signals for the same area and times.

During the 1993 field season, thermocouples and thermistors were used to measure a vertical temperature profile at the research camp from May 29 through June 19. The instruments, which were calibrated in Greenland in a 0° C ice bath, were placed at various depths ranging from 2.5 cm below the surface to 196 cm below the surface, the snow/ice interface. Manual temperature measurements were made near the surface using four Fluke 80PK-2A type K thermocouples. These measurements, which were made at 2.5, 5, 10, and 20 cm (probes 1 - 4 respectively), had to be made manually in order to avoid instrument solar heating effects which would occur if they were continually taking readings due to their proximity to the surface. Probes 5 - 10, which were Campbell Scientific model 105 thermocouples, were placed below the surface at depths of 25, 28, 32, 37, 42, and 49 cm respectively, and probes 11-15, which were Campbell Scientific model 107 thermistors, were placed at depths of 60, 77, 102, 140, and 196 cm respectively. The thermocouples monitored the average temperatures at 1 hour intervals. Finally, surface temperature measurements were taken with an Everest Scientific Model 110 infrared thermal gun.

With these measurements, the diurnal cycle, as well as the response of the snow to the seasonal temperature increase, were monitored with respect to depth. The results of these measurements are shown in Figure 4.1. The figure illustrates the reduction in magnitude of the diurnal cycle both with depth and with the approach of the melt period. Also evident is the time lag for the melt onset between the surface thermocouples, and the ones at greater depths. The sustained melt near the surface began on June 9 (Julian Day 160) while the onset of melt at the greater depths occurs later (e.g. nine days later at probe #10). Melt at the snow/ice interface never occurred during our field season. These relationships are of critical importance to the determination of a multispectral algorithm for snow melt characterization, because they can be related to signal changes due to the different penetration depths of the different channels.

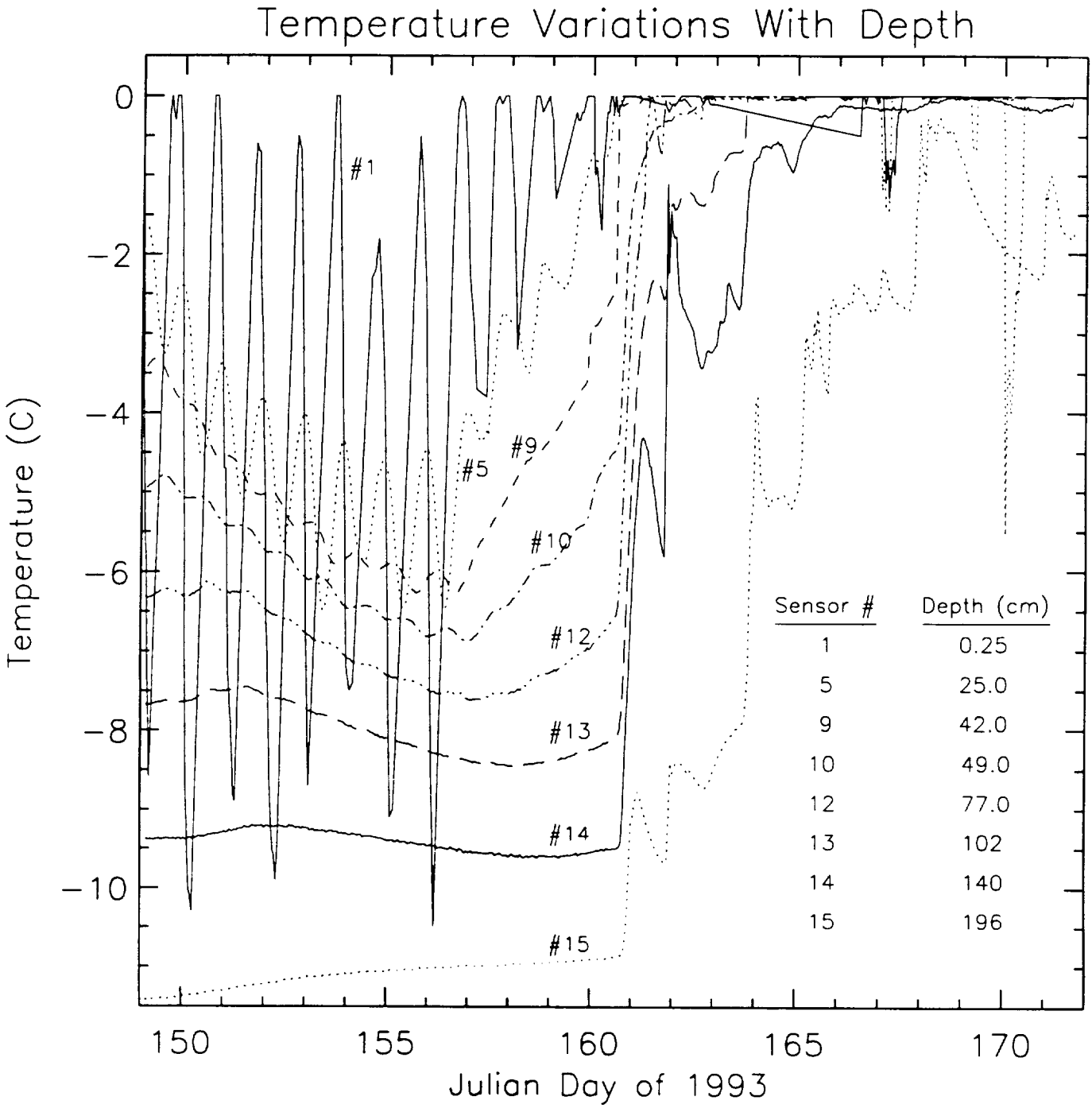

Figure 4.1 Snow temperature record.

4.2 Conductive Heat Flux

Using the temperature profile data along with density measurements which were taken in the field, a model was constructed which describes the heat flux for the entire surface snow thickness. For modeling purposes, the snow was divided into 10 continuous layers, and an energy balance was done for each layer according to the following equation:

$$Q(out) = Q(in) + Q(stored) + Q(phase\ change)$$

That is to say that the energy that leaves (or enters) the top of a layer is equal to the sum of: 1) the energy that enters (or exits) the bottom of a layer, 2) the heat stored which changes the temperature in the layer, and 3) the heat absorbed or released during snow phase change. Using this model the heat fluxes were determined for each layer, and the flux at the top boundary of the top layer was taken as the ground flux in the surface energy balance.

The calculation of this ground flux from direct temperature measurements in the snow is necessary for comparison to the ground flux derived with the eddy correlation method (see section 4 below), because the latter is a residual value (i.e. it is not directly measured); therefore, it has the cumulative uncertainty of all of the other measurements. The ground flux, calculated with both methods, is shown in Figure 4.2.

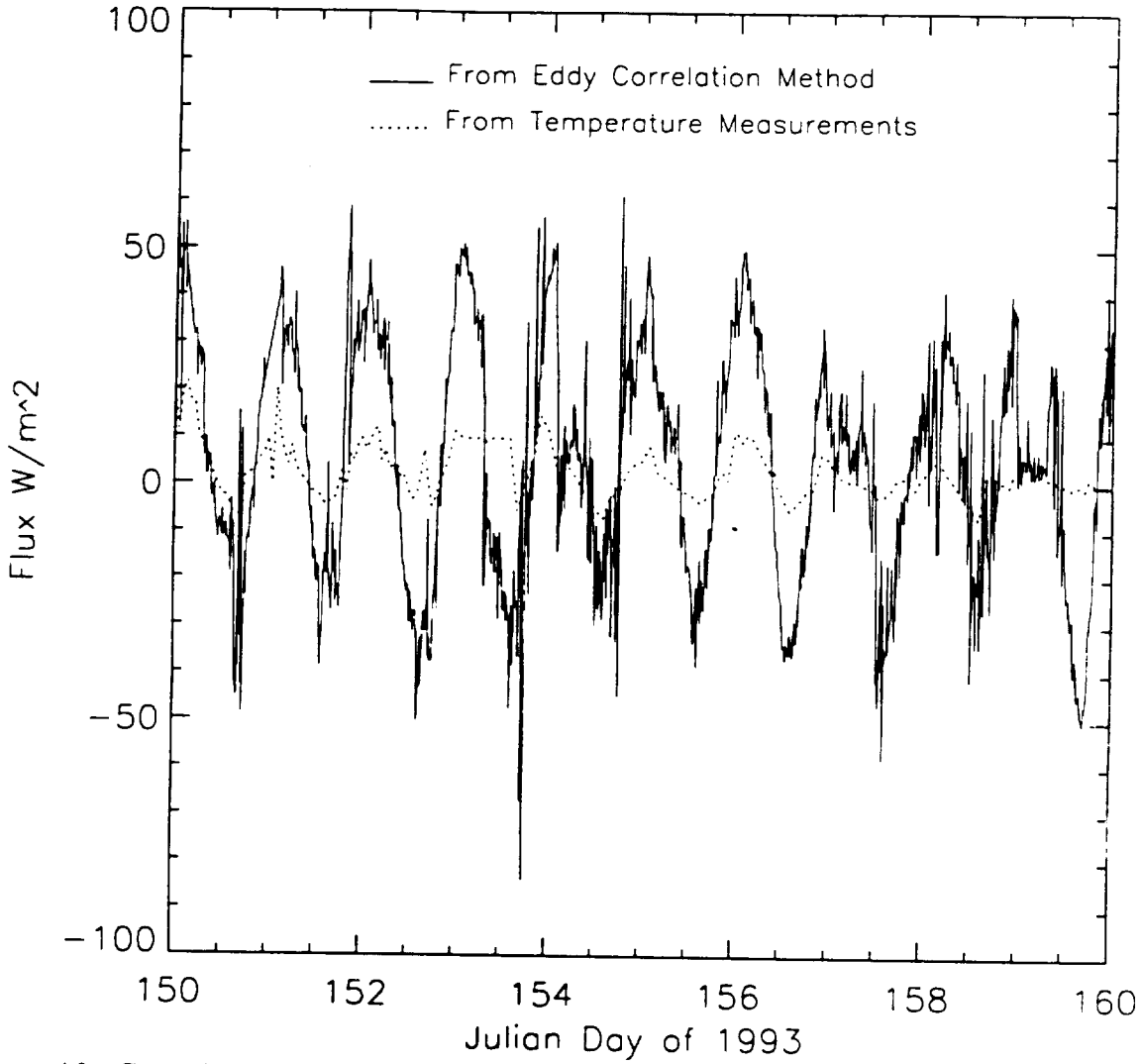

Figure 4.2 Ground heat flux comparison. Positive indicates a net flux out of the ground, and negative indicates net flux into the ground.

The two methods agree well in terms of their representation of the heat flux trends, however, they differ considerably in magnitude, often by up to 40 Wm^{-2}. The conductive heat flux derived as a residual from eddy correlation method has a mean value of -1.9 Wm^{-2} and the ground heat flux derived from the temperature probes has a mean value of 1.5 Wm^{-2}. Assuming that the cumulative errors are represented by the discrepancies between the two calculations, the fact that the error for individual measurements is generally within 40 Wm^{-2} is encouraging.

4.3 Correlation Between in situ and Passive Microwave Data.

As mentioned above, the passive microwave emittance has a distinct melt signature which is due to the presence of water in the snow. This water significantly increases the effective emissivity of the snowpack. Although the signature exists in all channels and both the horizontal and vertical polarizations, the gradient ratio, defined by:

$$GR = [T_b(19GHz)-T_b(37GHz)]/[T_b(19GHz)+T_b(37GHz)]$$

where T_b = brightness temperature, is most useful in detecting melt regions for two reasons: 1) It is unaffected by physical temperature of the snow; thus a threshold can be defined without considering temperature variations, and 2) the onset of melt, as the melt depth increases, is more accurately described by the combination of two channels as opposed to a single channel.

Figure 4.3 shows a time series of horizontally polarized gradient ratios for the period January, 1988 through March, 1991. The onset of melt is characterized by the slight dip in gradient ratio around April or May. This dip is due to the different penetration depths of the 37 GHz and 19 GHz channels. The melt at the surface comprises a larger component of the 37 GHz signal than it does in the 19 GHz signal, Thus the 37 GHz brightness temperature shows a significant increase before the 19 GHz brightness temperature does. Consequently, the resulting gradient ratio decreases at the onset of melt.

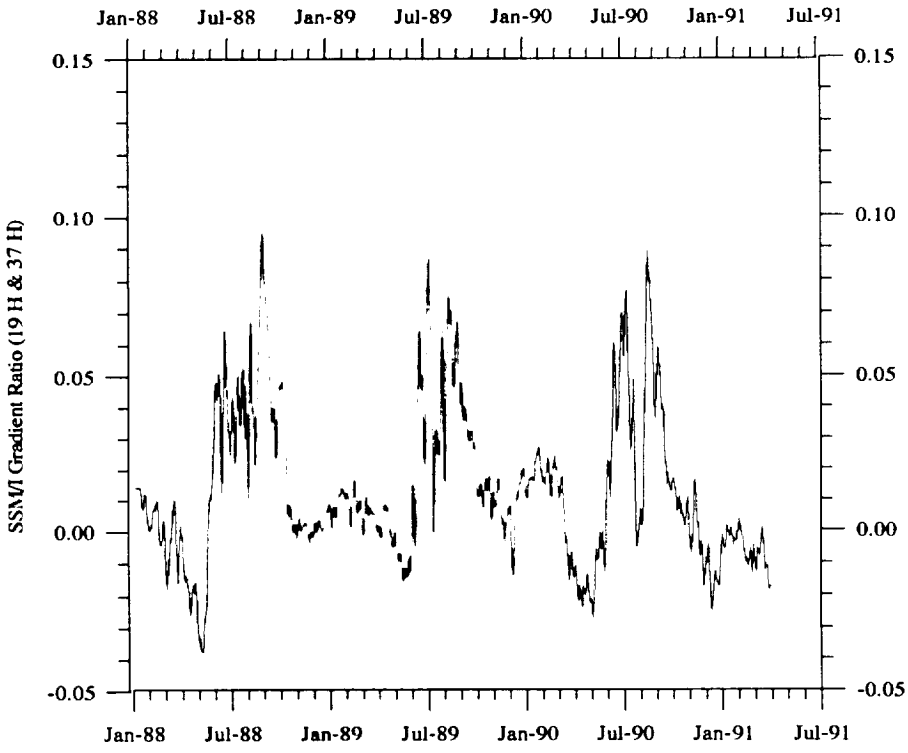

Figure 4.3 SSM/I Gradient Ratio time series

Unfortunately, the SSM/I data for the period of coverage from this year's field season are not yet available. However, a comparison between SSM/I data and field data for a previous year, 1991, shows that for a gradient ratio threshold defined at GR=0.025, the melt occurrence is consistent with increase of air temperature in the region to above freezing (Steffen et al. 1993). This threshold is shown in Figure 4.3.

Using GR=0.025 as the threshold value, the entire ice sheet was examined for periods of one week in the middle of each month of the 1990 summer. Areas that exhibited gradient ratios in excess of 0.025 were classified as wet, while those that did not, were classified as dry. The results of this classification are shown in Figure 4.4. The initial calculations indicate that in 1990, the maximum wet snow extent was 26% of the ice sheet (Steffen et al. 1993).

When the SSM/I data that correspond to the 1993 field season become available, the threshold will be more accurately defined and the entire passive microwave data set will be examined to produce biweekly melt maps.

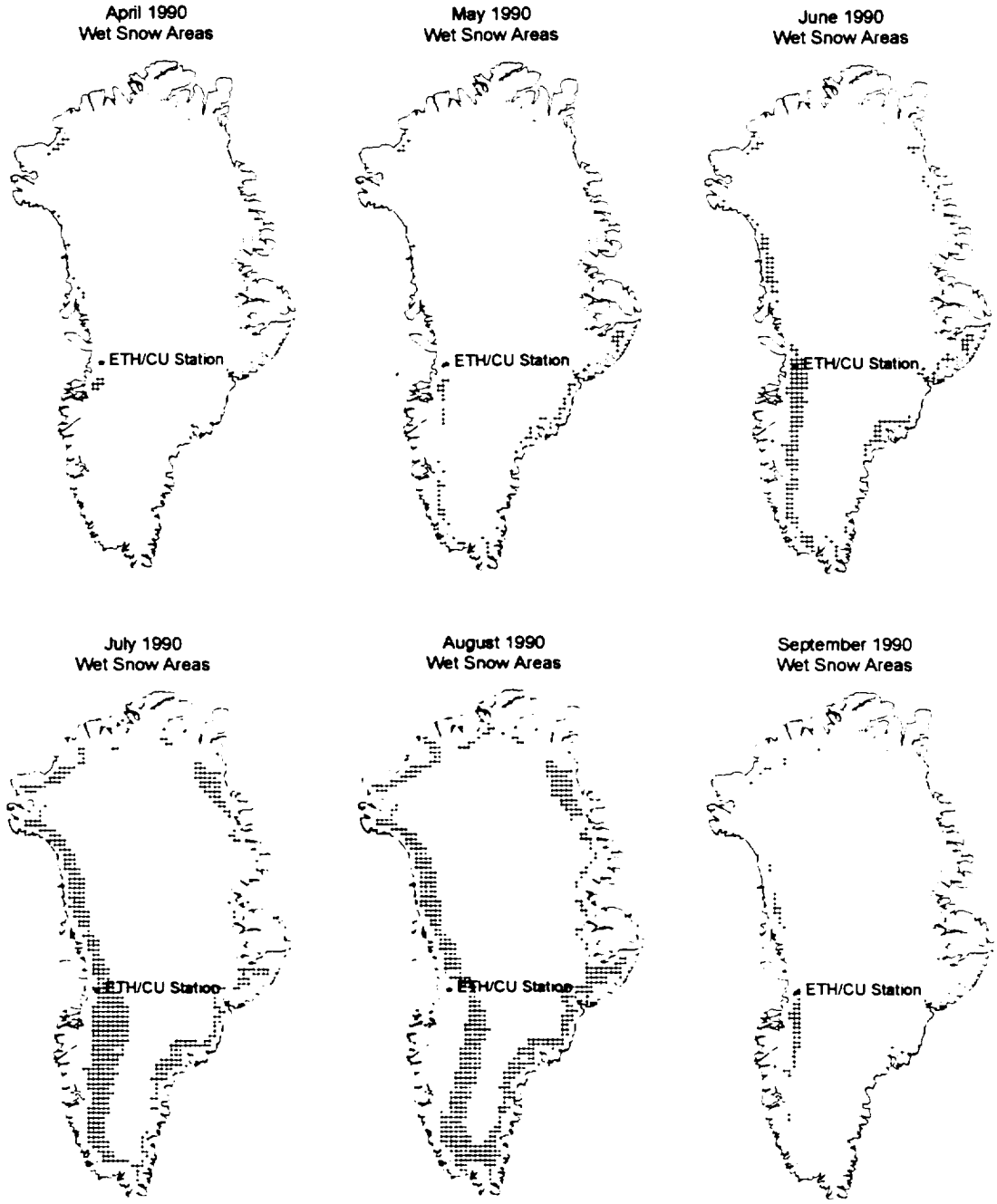

Fig. 4.4 Wet snow areas of the Greenland Ice Sheet for 1990

5. SNOW ACCUMULATION ESTIMATES

An understanding of changes in the mass balances on the ice sheets of the world can provide important insight to changes in global climate. One of the most significant components of these mass balances is the annual snow accumulation on the ice sheets. For this reason, we are currently investigating a means of assessing these accumulation rates on large scales using passive microwave satellite data.

5.1 Radiative Transfer Modeling of the Polar Firn

There have been observed temperature trends throughout most the dry snow areas of Greenland (Fig. 5.1). The strength of these trends seems to vary inversely with mean accumulation rates; i.e. the areas with the lowest accumulation rates, (northeast Greenland) exhibit the strongest temperature trends, and visa versa. Thus it has been inferred that the amount that snow accumulation rate variations affects the brightness temperature is dependent on the relative contribution of larger particles from previous years' snow, and the smaller particles from the current year's snowfall. Increases in snow accumulation rates result in a greater contribution from the smaller newer particles, which then increases the emissivities and brightness temperatures. Conversely, decreases in accumulation rates result in a greater contribution from the old snow, and subsequently reduce the brightness temperature.

These relationships were investigated by Zwally (1977), but to understand more fully how they apply to the SMMR and SSM/I signals over Greenland, a model using the discrete ordinate radiative transfer code (DISORT) has been constructed to represent the polar firn. The model is a multiscattering, slab geometry model which was set up to represent the 19 GHz channels. The Mie/Rayleigh scattering coefficients, as well as the expressions for optical depths and single scattering albedos, were obtained from Zwally (1977). As was the case with the snow grains, the depth hoar particles were assumed to be spherical and independent scatterers. The depth hoar size variation with changing accumulation rates was represented by the following formula:

$$r = r_0 \, (2A)/(A+(z_1-z_2))$$

where r is the varying particle radius, r_0 is the particle radius for the mean annual accumulation, A is the mean annual accumulation (cm), and (z_1-z_2) represents the difference in height of the current years snow from the mean (cm).

The model has six different layers: The top layer represents the current years' snowfall, and was made to vary in accordance with different accumulation rates. The second, which was held at 1 cm thickness, was used to describe the hoar layer between current and previous year's snow. The remaining layers represented old snow of varying particle size. The emissivities were calculated by running the model first for the case described by the model parameters taken from Zwally (1977) and again by running the model for snow as a black body (i.e. setting the single scattering albedo to zero). The grey body radiance was then divided by the black body radiance and the resulting quotient is the emissivity.

Initially the model was run for a varying temperature/depth profiles as well as an isothermal case. The temperature data for the varying conditions were calculated from the formula for Maudheim (71° N and 10.5° W) given in Zwally (1977, eq. 43). The results showed that the temperature gradient has a maximum impact of 0.5% on calculated emissivity; therefore, all subsequent model runs were made for an isothermal medium.

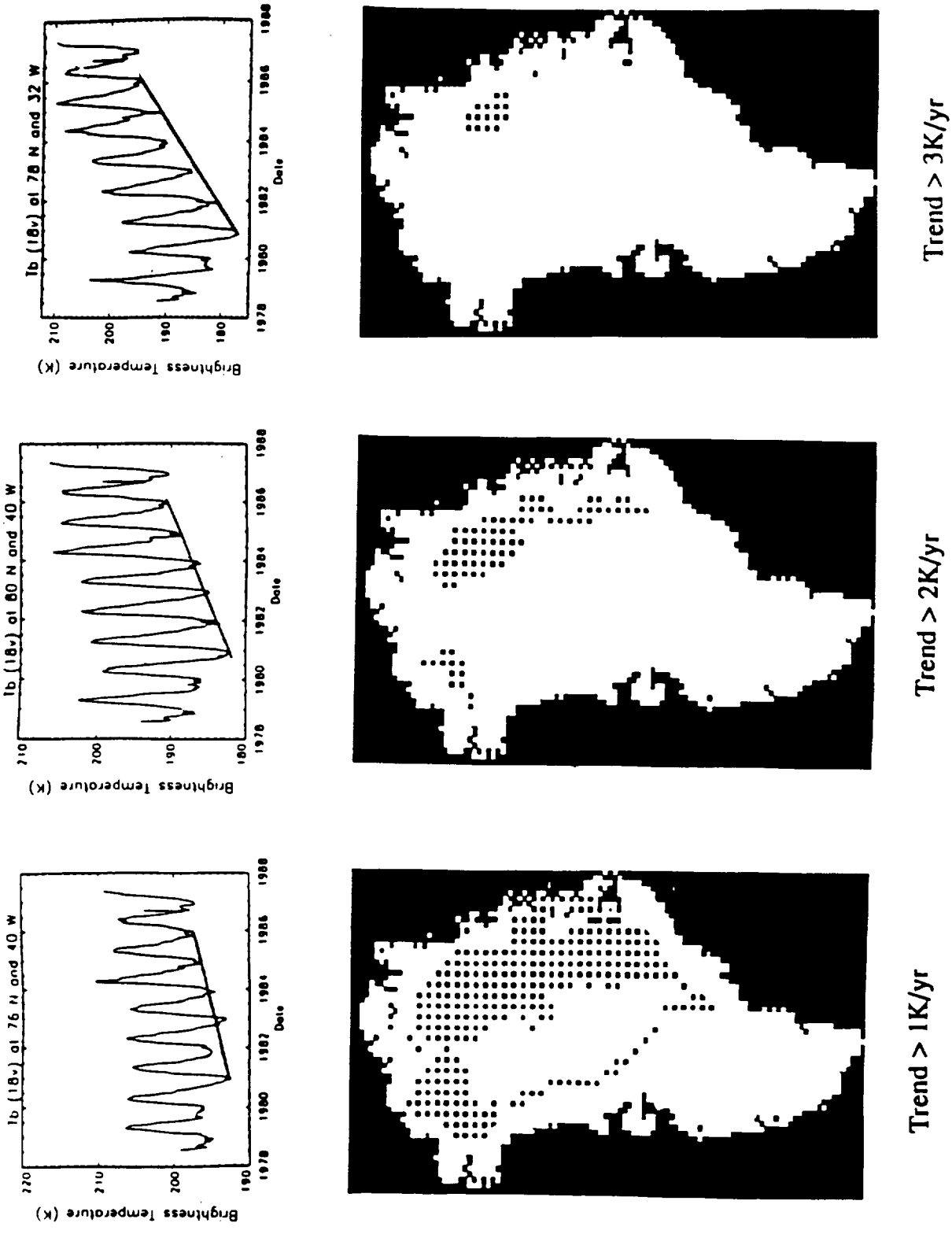

Fig. 5.1 *Brightness temperature trend areas throughout Greenland*

The model results are shown in Figures 5.2 and 5.3. Fig. 5.2 shows the case without depth hoar. It is important for two reasons: The first is that it easily enables the calculation of percent contribution from new snow to the microwave signal by taking the difference between emissivity for any given accumulation rate and the emissivity for the zero accumulation rate and then dividing that difference by the difference between the emissivities for infinite and zero accumulation rates. Using this relationship, it appears that nearly all of the signal is emitted from the current year's snow, when the snow depth is approximately 5m. This is consistent with previous calculations for 19 GHz (Chang et al. 1976).

The second reason is that it indicates that in the 30 cm mean annual accumulation areas (where the observed brightness temperature trend was approximately 3° Ky^{-1}), a change in accumulation rate of 33% (10 cm) results in a brightness temperature change of approximately 1.1° K. This relatively weak relationship, which is even weaker for the 60 cm mean accumulation, indicates that there is an additional factor which contributes to the trends; the dry snow accumulation changes are not enough. Based on the radiative transfer model results, we believe this additional factor is the depth hoar.

Figure 5.3 shows the model results for a case without depth hoar, a case with two millimeter diameter depth hoar particles, and a case with 3 mm diameter depth hoar particles. It is obvious that cases which include depth hoar show a stronger sensitivity (i.e. a greater slope in the graph), in the 30 cm mean annual accumulation region to changes in accumulation, than cases where the mean annual snowfall is twice as much, or greater. This is because the depth hoar scattering reduces the signal contribution from the deeper snow and effectively increases the signal contribution from the fresher snow.

5.2 Results for the Greenland Ice Sheet

This sensitivity relationship corresponds well to the trends observed in the Greenland brightness temperature data. As stated above, the trends were strongest in the northeast region where accumulation rates are lowest (Fig. 5.1), approximately 100 mm water equivalent per year (Ohmura and Reeh, 1991), which corresponds roughly to 30 cm of snow annually. Trends are weak, in fact they are not really evident, in the areas where snow accumulation exceeds 90 cm annually.

Based on the assumption that it is the accumulating snow that is responsible for the trends (Steffen et al. 1993), the satellite observations are consistent with the model calculations in the presence of depth hoar. Though the relationship is only qualitative at this point, we expect that using multiple channels, we expect to be able to provide quantitative estimates of the accumulation rates.

5.3 Results for Antarctica

A preliminary examination of Antarctica for brightness temperature trends in excess of 1° K per year over the SMMR coverage period only shows such trends to be apparent on the ice shelves and near the coasts (Fig. 5.4). A possible explanation for the relative absence of trends in the other regions is that the low temperatures result in a very small particle size gradient, which in turn results in little variation in brightness temperature with accumulation rate changes. On the ice shelf, the scattering from the ice below the snow is so high, that the signal is comprised primarily of the snow that sits on top of the ice shelf. Thus accumulation changes have more impact on the signal.

Another explanation may be due to the small particle size itself. Since the temperatures are colder, the particle sizes are smaller, and therefore, the penetration depth is greater. The greater penetration depth results in an effective signal contribution from greater depths; consequently, changes at the surface have less impact on the signal.

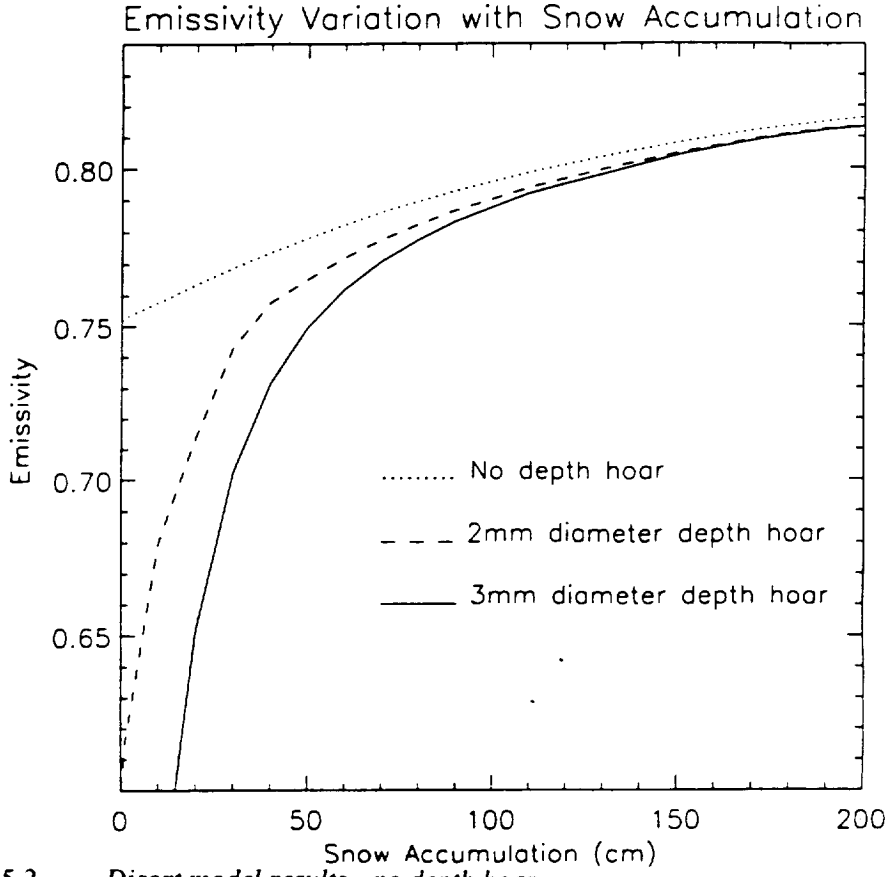

Figure 5.2 ***Disort model results - no depth hoar***

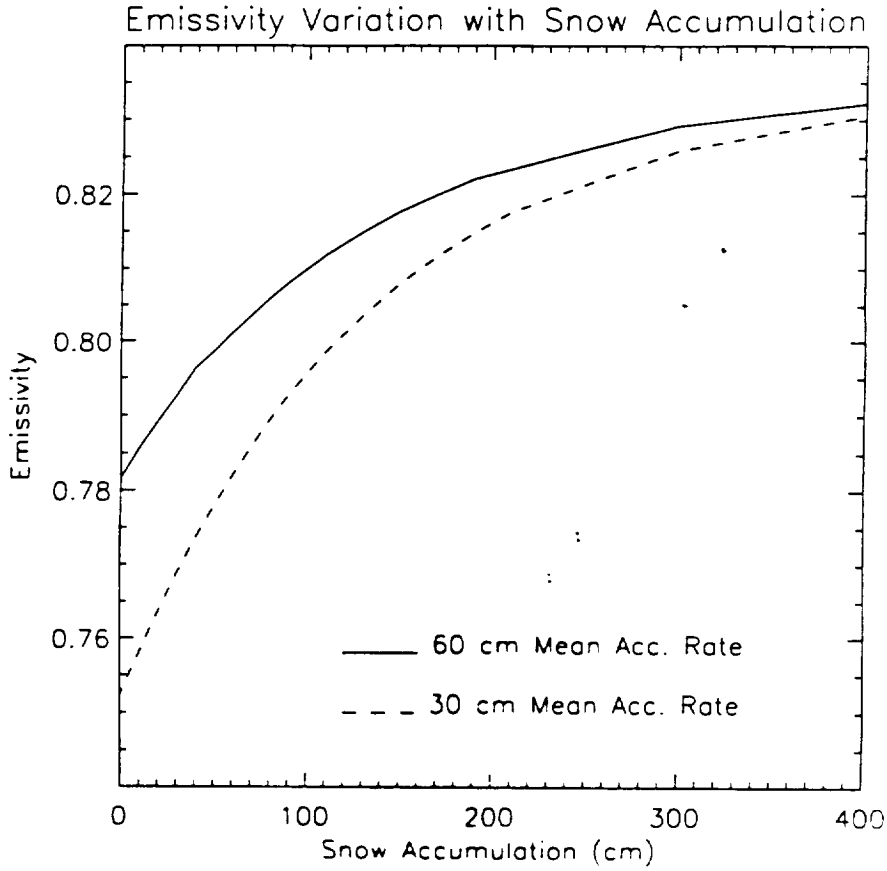

Figure 5.3 ***Disort model results - including depth hoar***

A final possibility is that the trends observed may in some way be an artifact of the melt cycle, and there may in fact be no appreciable accumulation change throughout all of Antarctica. The extent of melt in Antarctica has not been assessed yet, but when it is, this issue will be addressed. The physical situation will be more closely examined after the relationships for Greenland are better established. The use of additional channels, and dual polarization will provide more information.

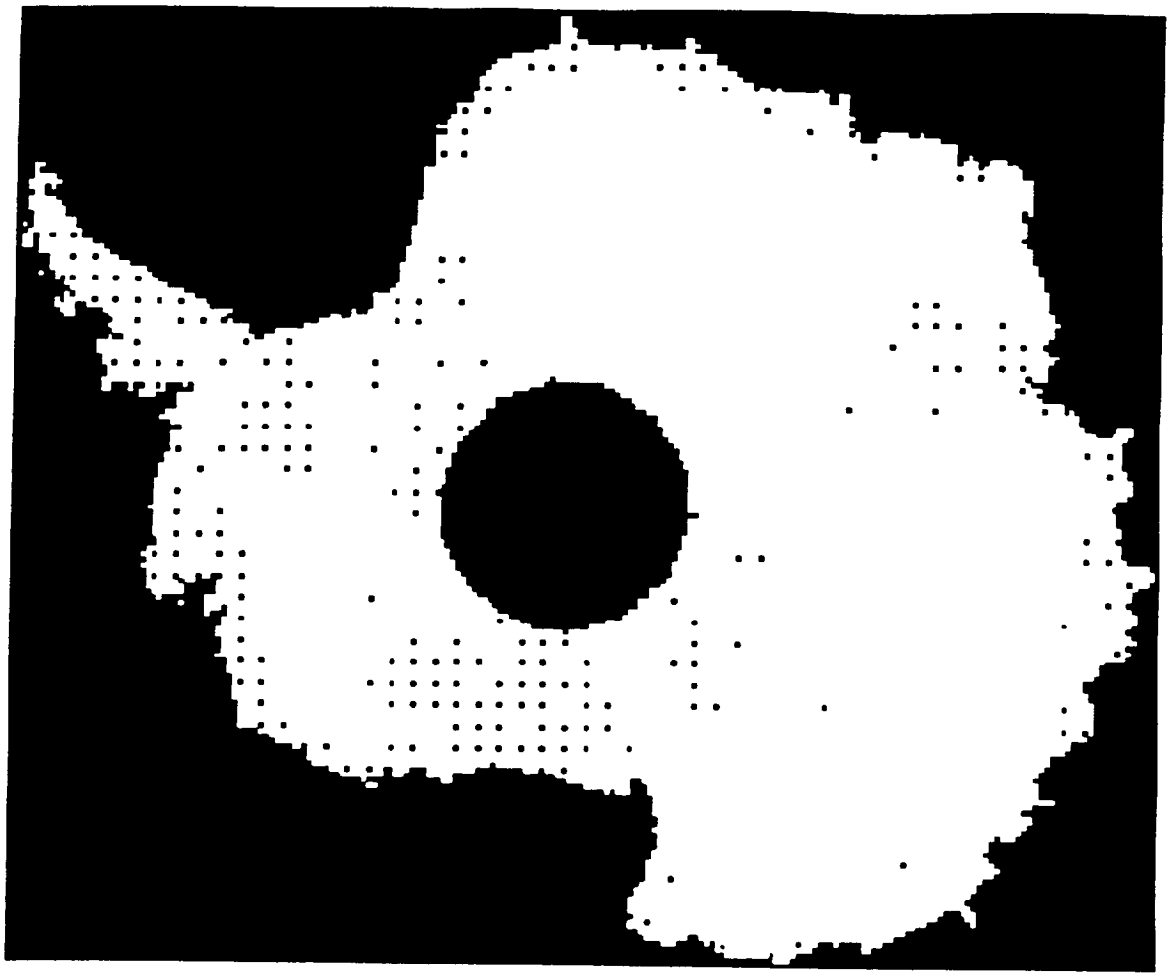

Figure 5.4 Antarctic regions with average temperature trends of 1° Ky^{-1}

6. OUTLOOK

The 1994 field season will have two components: a dry snow component and a wet snow component with critical attention paid to properties of the snow throughout the transition from one to another. Like last season, temperature variations with depth will be closely monitored along with snow density and wetness conditions, These parameters will be related to the satellite signal in order to improve the wet snow classification threshold. Additionally, since the snow grain size also impacts the passive microwave melt signature, variations in these grain sizes with depth and through the melt period will be studied as well.

6.1 Surface Energy balance

Further, the field measurements for 1994 will include an integrated measurements of surface energy balance, spectral bidirectional reflectance, snow grain size distributions, soot concentrations, and liquid water generation and movement in the snowpack. In this way, we will be able to relate changes in spectral reflectance with snowpack energy balance. As in the previous field season, the heat transfer in the snow will be calculated from the temperature and density measurements, These will be related the residual heat flux calculated using the eddy correlation method for a more accurate assessment of the surface energy balance.

6.2 Snow grain size

Of particular interest is characterization of the snow grain size distribution for both the optical and microwave regions and examination of changes in the grain size distribution over time. Snow spectral reflectance measurements will be made using a full-range (0.4 - 2.5 μm) field spectrometer and data will be regularly collected for series of angular reflectance measurements over a wide range of solar zenith angles and for a variety of snow conditions. Soot concentrations will be measured by collecting snow samples in the upwind vicinity of the field station; samples will be brought back to the University of Colorado for laboratory analysis using a particle counter.

Grain size distributions will be obtained using a serial sieving method combined with photomicrography of the snow grains. Photomicrographs provide a means of documentation of the grain sizes and allow us to use digital analysis techniques for snow grain characterizations. In situ measurements of snow bulk density profiles will be acquired to further characterize the snowpack. Movement of liquid water in the snowpack will be monitored using a series of dye tracer experiments in which dye placed on the snowpack surface is carried down through the snowpack mapping the circuitous routes of water movement. This process is documented by photographing snowpit profiles in which the dye is visible.

6.3 Microwave penetration

Also, this year we will be taking a C-band active radar developed by P. Gogenini at the University of Kansas to monitor the change in penetration depth as the snow wetness increases. Such a study will be of use to us in understanding the depth from which the microwave signal is emitted for varying degrees of wetness. All of the above mentioned properties are of great importance in translating the observed satellite signal into meaningful information about the snow and climate conditions.

6.4 Atmospheric optical depth

Satellite measurements are also affected by atmospheric scattering and absorption, by the various combinations of sun-target-sensor geometry, and by clouds. Derivation of surface albedo from satellite data is further complicated by the limited number of clear views, by limited sampling of the complete sun-target-sensor geometry, and by the time variation of the atmospheric constituents and surface properties. In order to correct for the intervening atmosphere, we need to parameterize the optical depths due to gases such as water vapor and ozone as well as the aerosol optical depth. To do this we intend to use a sun photometer

mounted on a solar tracker to measure the direct solar irradiance selecting wavelength intervals in the visible (aerosols), near infrared (water vapor), and a pair of wavelengths in the Hartley-Huggins ozone absorption band. Measurements will be made throughout the day in order to infer the diurnal variation of these atmospheric constituents. At the same time surface albedo will be measured, and accurate observations of clouds will be made.

6.5 Satellite link

At the end of the field season we will install a microwave satellite link that will enable us to broadcast the climatological data on a daily basis via the geostationary satellite to the US For the first time we will try to measure the accumulation rate of the winter snow precipitation based on a air thermistor chain and the longwave incoming radiation in addition to the 25 climate parameters already recorded on an hourly basis.

6.6 Geodetic programme

We will also host two German visiting scientist at the CU/ETH camp from the Engineering school of Surveying (Prof. M. Stober and his assistant). They will continue their geodetic program they started during the 1991 field season on our camp. A very important part in determining the volume of the ice is the knowledge of the surface heights and their temporal change. The German research team will operate high resolution Global Positioning Systems. The intention of the research is to examine more closely the refraction under the special conditions over the Greenland ice surface. Knowledge of the related meteorological parameters is absolutely necessary and therefore, collaboration with the ongoing climate study is very beneficial

7. REFERENCES

Baldwin, D., and W.J. Emergy, A systematic approach to AVHRR image navigation, *Annals of Glaciology*, 17, 414-420, 1993.

Chang, T. C., P. Gloerson, T. Schmugge, T.T. Wilheit, and H.J. Zwally, Microwave emission from snow and glacier ice, *J. of Glaciology*, 16(74), 23-39, 1976.

Edlen, B., The refractive index of air, *Meteorol.*, 2, 71-80, 1966.

Haefliger, M., K. Steffen and C. Fowler, AVHRR surface temperature and narrow-band albedo comparison with ground measurements for the Greenland Ice Sheet, *Annals of Glaciology*, 17, 49-54, 1993.

Iqbal, M., An Introduction to solar radiation, *Academic Press*, Toronto, pp.380, 1983.

Kidwell, K.B., NOAA Polar Orbiter Data Users Guide, NOAA Information Service and Climate Data Center, Satellite Data Service Division, Washington D.C., 1991.

Koepke, P., Removal of atmopsheric effects from AVHRR albedos, J. *Appl. Meteorology*, 28, 1341-1348, 1989.

Li, Zhanqing, and H.G. Leighton, Narrow-band to broad-band conversion with spatially autocorrelated reflectance measurements, *J. of Applied Meteorology*, 31(5), 421-430, 1992.

Lindsay R., and D. Rothrock, The calculation of surface temperature and albedo of Arctic sea ice from AVHRR, *Annals of Glaciology*, 17, 391-396, 1993.

Ohmura, A., and N. Reeh, New precipitation and accumulation maps for Greenland. *J. of Glaciology*, 37(125), 140-148, 1991.

Orvig, S., Climate of the polar regions, *World Survey of Climatology*, 14, Elsevier Publishing Company, New York, 1970.

Penndorf, R., Talbes of the refractive index for standard air and the Rayleigh scattering coefficient for the spectral region between 0.2 and 20.0 microns and their application to atmospheric optics, *J. Opt. Soc. Am.* 47, 176-182, 1957.

Steffen, K., W.Abdalati, and J. Stroeve, Climate sensitivity studies of the Greenland Ice Sheet using satellite AVHRR, SMMR SSM/I and in situ data, *Meteorology and Atmosph. Physics*, 239-258, 1993.

Tanre, D., and P. Duhaut, Description of a computer code to simulate the satellite signal in the solar spectrum: the 5S code, *Int. J. Rem. Sens.*, 11, 659-688, 1990.

Wydick, J. E., A.D. Paul, and A. Gruber, Estimation of Broad-band Planetary Albedo from Operational Narrow-band Satellite Measurements, NOAA Technical Report NESDIS 27, April 1987

Young, A. T., Revised depolarization corrections for atmospheric extinction, *Appl. Opt.* 27, 3427-3428, 1980.

Zwally, H. J., Microwave emissivity and accumulation rate of polar firn, *J. of Glaciology*, 18(79), 195-216, 1977.

8. Presentations and Publications Supported by NAWG-2158

8.1 Presentations

Abdalati, W., K.Steffen, and J.Stroeve, Application of passive microwave satellite data to climate studies on the Greenland Ice Sheet, Colloquim, Colorqado Center for Astrodynamic Research, Boulder, 31 March, 1993.

Abdalati, W., K. Steffen, and J. Stroeve, Detection of changes in snow accumulation on the Greenland Ice Sheet using passive microwave satellite data, AGU Fall Meeting, 6 Dec., 1993.

Steffen, K., J. Stroeve, W. Abdalati, Surface processes at the equilibrium line altitutde of the Greenland Ice Sheet and its application to satellite measurements, AGU Fall Meeting, 6 Dec., 1993.

Steffen,K., Greenland Ice Sheet and climate interaction (invited talk), McGill University, Department of Meteorology Seminar, March 3, 1993.

Steffen, K., The Greenland climate initiative at the University of Colorado at Boulder, US Arctic Research Consortium, the Arctic Forum, University of Wisconsion in Madison, 21-22 March, 1993.

Steffen, K., J. Stroeve, W. Abdalati, Evidence of global climate change? Case study: Greenland, 3rd Global Change end Environmental Quality Symposium, University of Colorado, Boulder, 29 April, 1993.

Steffen, K., Climate sensitivity analysis of the Greenland Ice Sheet, Colloquim, Geography Department, University of Colorado, Boulder, 12 Nov., 1993.

Steffen, K., Remote sensing opportunities for ice sheet mass balance determination, Ice Sheet-Climate Interaction Workshop, European Committee on Ocean and Polar Science, Aghia Pelaghia, Crete, Greece, 17-22 Sept., 1993.

Steffen, K., Shortwave radiation and albedo, NASA Datra Workshop, Seattle, 3-4 Nov., 1993.

Stroeve, J., K. Steffen, W. Abdalati, Accuracy assessment of AVHRR broad-band albedo as derived over the Greenland Ice Sheet, AGU Fall Meeting, 6 Dec., 1993.

8.2 Workshops Proceedings

Abdalati, W., K. Steffen, and J. Stroeve, Detection of Chnages in snow accumulation on the Greenland Ice Sheet using passive microwave satellite data, 1993 AGU Fall Meeting, EOS Transactions, 74(43), 246, 1993.

Steffen, K., J. Stroeve, W. Abdalati, Surface processes at the equilibrium line altitutde of the Greenland Ice Sheet and its application to satellite measurements, 1993 AGU Fall Meeting, EOS Transactions, 74(43), 246, 1993.

Steffen, K., J. Stroeve, W. Abdalati, Evidence of global climate change? Case study: Greenland, 3rd Global Change end Environmental Quality Symposium, University of Colorado, Boulder, April 29, symposium Abstracts, p.30, 1993.

Stroeve, J., K. Steffen, W. Abdalati, Accuracy assessment of AVHRR broad-band albedo as derived over the Greenland Ice Sheet, 1993 AGU Fall Meeting, EOS Transactions, 74(43), 246, 1993.

8.3 Publications

Haefliger, M., K. Steffen and C. Fowler, AVHRR surface temperature and narrow-band albedo comparison with ground measurements for the Greenland Ice Sheet, *Annals of Glaciology*, 17, 49-54, 1993.

Steffen, K., W.Abdalati, and J. Stroeve, Climate sensitivity studies of the Greenland Ice Sheet using satellite AVHRR, SMMR SSM/I and in situ data, *Meteorology and Atmosph. Physics*, 239-258, 1993.

Steffen, K., R. Bindschadler, J. Comiso, E. Eppler, F. Fetterer, J. Hawkins, J. Key, D. Rothrock, R. Thomas, and R. Weaver, Snow and ice applications of AVHRR in polar regions, *Annals of Glaciology*, 17, 1-16., 1993.

Steffen, K., AVHRR applications for sea ice and surface studies, Book chapter CRC Press INC., in press.